THE JOURNAL OF PHYSICAL CHEMISTRY LETTERS
A JOURNAL OF THE AMERICAN CHEMICAL SOCIETY

pubs.acs.org/JPCL

Letter

Photoinduced Transition from Quasi-Two-Dimensional Ruddlesden–Popper to Three-Dimensional Halide Perovskites for the Optical Writing of Multicolor and Light-Erasable Images

Sergey S. Anoshkin, Ivan I. Shishkin, Daria I. Markina, Lev S. Logunov, Hilmi Volkan Demir, Andrey L. Rogach, Anatoly P. Pushkarev,* and Sergey V. Makarov*

Cite This: *J. Phys. Chem. Lett.* 2024, 15, 540–548

Read Online

ACCESS | Metrics & More | Article Recommendations | Supporting Information

ABSTRACT: Optical data storage, information encryption, and security labeling technologies require materials that exhibit local, pronounced, and diverse modifications of their structure-dependent optical properties under external excitation. Herein, we propose and develop a novel platform relying on lead halide Ruddlesden–Popper phases that undergo a light-induced transition toward bulk perovskite and employ this phenomenon for the direct optical writing of multicolor patterns. This transition causes the weakening of quantum confinement and hence a reduction in the band gap. To extend the color gamut of photoluminescence, we use mixed-halide compositions that exhibit photoinduced halide segregation. The emission of the films can be tuned across the range of 450–600 nm. Laser irradiation provides high-resolution direct writing, whereas continuous-wave ultraviolet exposure is suitable for recording on larger scales. The luminescent images created on such films can be erased during the visualization process. This makes the proposed writing/erasing platform suitable for the manufacturing of optical data storage devices and light-erasable security labels.

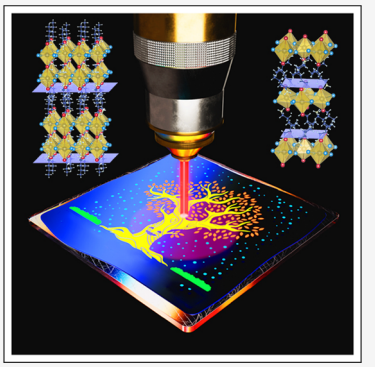

As powerful tools for the manipulation of big data, state-of-the-art technologies enabling the recording of information at nano- and microscales are expected to accelerate progress in natural sciences and medicine.[1−5] Also, it would be profoundly beneficial if such a new technology were not only to afford huge capacity for data storage but also to enable devices with high-level security anticounterfeit labels. From this point of view, optical data writing applied to luminescent materials such as lead halide perovskites (LHPs) could offer solutions.[6−9] The writing process should, however, be a high-throughput and well-controlled process, but at the same time hard to reproduce, without having full knowledge of the specific process.[10−12]

Bearing all of these points in mind, we believe that the choice of laser writing on solution-processed LHP thin films could be a viable option for addressing the demands. Indeed, the extremely low thermal conductivity (~0.5 W m^{-1} K^{-1}, which is less than that of silica glasses[13]) of ABX_3 [A = MA^+ (methylammonium), FA^+ (formamidinium), or Cs^+; B = Pb^{2+}; X = Cl^-, Br^-, or I^-] perovskites allows for high-density optical data writing,[8] as well as directly patterning laser microdisks, nanowire arrays,[7,14] and various micro-optical elements[15−17] obtained by laser ablation. Moreover, photoluminescence (PL) spectral tunability over the visible spectral range can be achieved for LHPs via partial or complete substitution of a certain anion (e.g., Br^-) for another one (e.g., Cl^- or I^-) at the X site.[18,19] Moreover, both photoinduced compositional and structural changes in the perovskite lattice could significantly impact its optical properties, as well. The former has been previously demonstrated for mixed-halide perovskites revealing a phenomenon of light-driven reversible anion segregation expressed in a PL red-shift upon illumination and its recovery in the dark,[20−22] whereas the latter is particularly true for the quasi-two-dimensional (quasi-2D) Ruddlesden–Popper (RP) phase undergoing dramatic changes in its structural and optical properties under intense photoexcitation.[23−25]

Importantly, the lead halide RP phase possessing an $A_2'A_{n-1}Pb_nX_{3n+1}$ structure [A′ is a large cation, e.g., BA^+ (*n*-butylammonium) or PEA^+ (phenethylammonium)] provides the possibility of tuning the PL spectrum with an additional degree of freedom owing to the quantum confinement phenomenon in thin $[PbX_6]^{4-}$ octahedral layers separated by A′ species in the perovskite stack,[26] whose thickness [i.e., number of octahedral layers (*n*)] is regulated by the ratio between the corresponding halide salts employed for the reaction. With respect to data storage applications, $(PEA)_2MA_{n-1}Pb_nI_{3n+1}$ phases (n = 1–5) were utilized to record information in resistive random access memory

Received: November 9, 2023
Revised: December 29, 2023
Accepted: January 3, 2024
Published: January 10, 2024

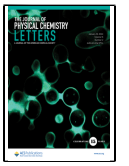

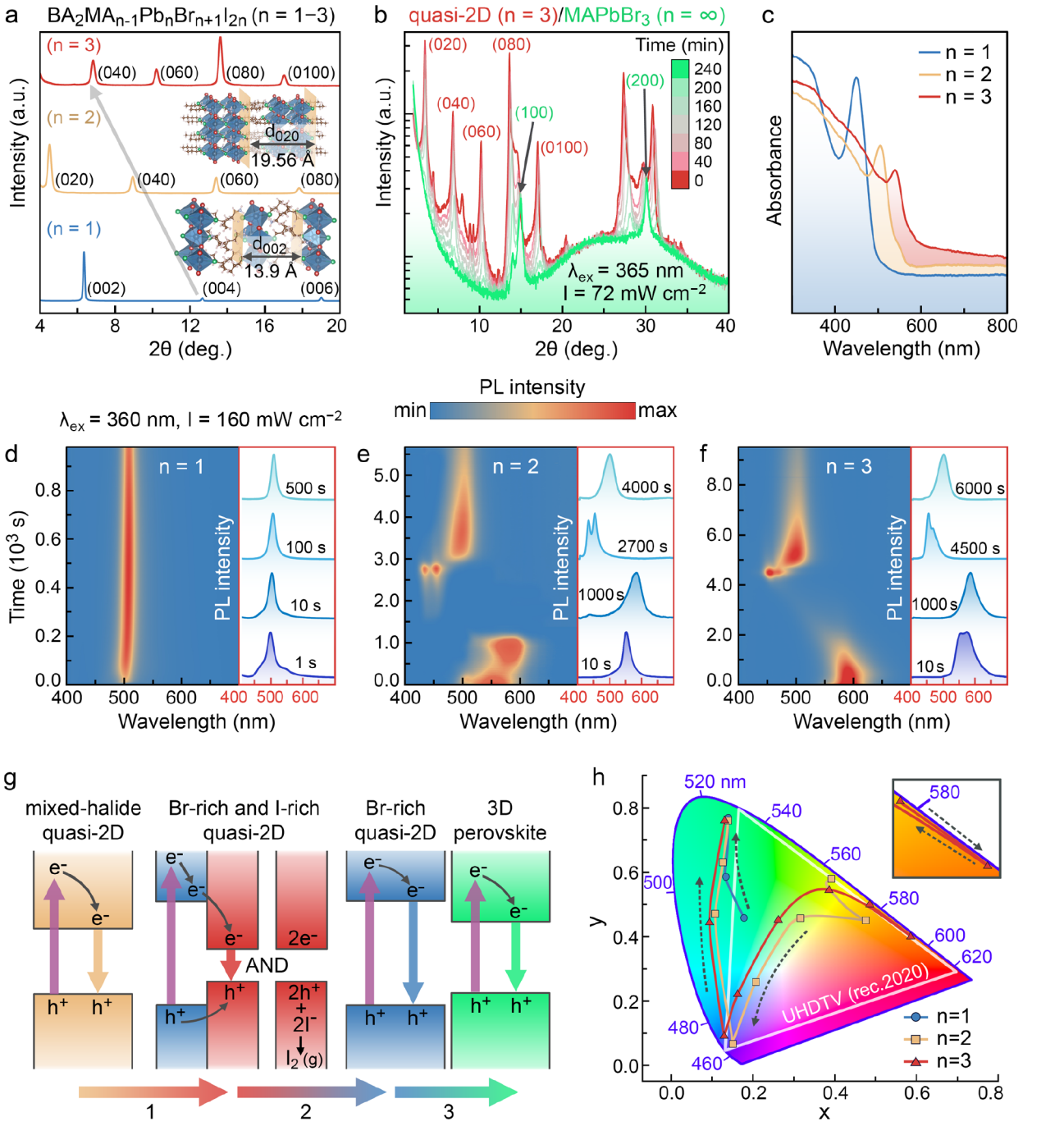

Figure 1. (a) XRD patterns of $BA_2MA_{n-1}Pb_nBr_{n+1}I_{2n}$ (n = 1−3) thin films. Insets illustrate the crystal structure and similar crystallographic planes for the n = 1 and n = 2 quasi-2D phases. The gray arrow shows an almost linear shift of the diffraction peaks toward smaller angles with an increase in the number (n) of $[PbX_6]^{4-}$ octahedral layers. (b) Data derived from *in situ* XRD measurements. According to the series of patterns, the n = 3 film undergoes a phase transition from the quasi-2D structure to bulk $MAPbBr_3$ (n = ∞) upon continious-wave UV excitation (I = 72 mW cm^{-2}) for 240 min. (c) Absorption spectra for the n = 1−3 RP films. (d–f) Evolution of PL spectra in the n = 1−3 films, respectively, exposed to 360 nm light with an intensity of 160 mW cm^{-2}. The n = 1 film shows exclusively green emission from the grain boundaries, whereas the n = 2 and n = 3 films demonstrate remarkable spectral tuning of the PL color. (g) Energy diagram depicting the possible mechanism for spectral tuning in the n = 2 and n = 3 films. Three types of compositional and structural transformation are indicated with gradient arrows: (1) light-induced halide segregation invoking Br- and I-rich quasi-2D phases, (2) I_2 release-assisted dissociation of the I-rich phase, and (3) sintering of the Br-rich quasi-2D phase resulting in the formation of the 3D bromide perovskite. (h) CIE 1931 color space showing the change in PL color corresponding to the dynamics plotted in panels d–f.

(ReRAM) devices.[27] In addition, it has been reported that the manipulation of light irradiation and gate voltage allows one to control the ion migration process and the current flow in a data storage device based on an ambipolar SnO transistor with a $(PEA)_2PbI_4$ photoactive layer[28] and, thus, to perform writing and erasing processes under illumination only. However, the use of lead halide RP phases, offering unique optical properties related to broadband spectral tunability for all-optical data storage and labeling, has not been reported to date.

https://doi.org/10.1021/acs.jpclett.3c03151
J. Phys. Chem. Lett. 2024, 15, 540−548

In this work, we systematically study the local optical response of mixed-halide RP phases $BA_2MA_{n-1}Pb_n(Br,I)_{3n+1}$ (n = 1−3) to light irradiation under ambient conditions and employ its tunability for the direct optical writing of various multicolor patterns with high resolution and broadband gamut. The quasi-2D structure of spin-coated perovskite thin films is confirmed by powder X-ray diffraction (XRD) and steady-state absorption spectroscopy. It is established that linear photoexcitation invokes almost no temporal change in the PL spectrum of the n = 1 film, whereas n = 2 and n = 3 films exhibit irreversible emission tunability in the range of 450−600 nm. The latter is explained by light-induced compositional and structural modification of the quasi-2D phases, which experience halide segregation and then the destruction of iodine-rich phases accompanied by I_2 release and thereafter undergo a phase transition toward the bulk $MAPbBr_3$ perovskite. The proposed mechanism for this observed optical response is in good agreement with *in situ* XRD measurements and tests demonstrating I_2 release. The larger the number of octahedral layers in the perovskite stack, the more resistant the RP phase is to the aforementioned light-driven modifications. Taking all of these findings into account, as a proof of concept, we employ the complex behavior of evolving PL under optical irradiation in the n = 3 film for two-photon direct laser writing (DLW) of high-resolution multicolor microimages, whereas simple projection ultraviolet (UV) lithography applied to the n = 2 film yielded luminescent labels, which can be erased by light during the reading process. The developed writing/erasing perovskite-based platform leverages cost-efficient synthesis and fabrication and can be employed for the manufacturing of optical data storage devices, information encryption, and security labeling.

Quasi-2D mixed-halide perovskite thin films with compositions of $BA_2PbBr_2I_2$ (n = 1), $BA_2MAPb_2Br_3I_4$ (n = 2), and $BA_2MA_2Pb_3Br_4I_6$ (n = 3) are obtained from 0.3 M solutions of PbI_2, methylammonium bromide (MABr), and/or *n*-butylammonium bromide (BABr) mixtures in anhydrous dimethyl sulfoxide (DMSO) spin-casted onto glass substrates, followed by annealing on a hot plate (for details, see Methods). The quasi-2D structure of the deposited films is confirmed by XRD measured in the Bragg−Brentano geometry (Figure 1a). Comparison of the recorded patterns with those reported by Stoumpos et al.[29] allows us to clearly identify the number (n) of $[PbX_6]^{4-}$ octahedral layers in the perovskite-like stacks. In the 2θ range of 4−20°, the first sample shows three peaks, among which the most intense one at 6.35° corresponds to the scattering of X-rays from (002) crystallographic planes confining a single octahedral layer and a double layer of the BA spacer cation. According to Bragg's law, the distance between the (002) crystallographic planes (d spacing) equals 13.9 Å, which is slightly shorter than that in BA_2PbI_4 [$d_{(002)}$ = 14.2 Å][29] because the mixed-halide counterpart possesses a more compact crystal lattice. Introducing one and two more octahedral layers along with a required amount of MA species into the perovskite unit results in the shifting of three diffraction peaks toward small angles and the appearance of additional peaks in the XRD patterns assigned to the (080) and (0100) planes, respectively (Figure 1a).

Because our study is focused on optical encryption, it is important to examine the structural evolution of any sample upon UV excitation. Therefore, *in situ* XRD measurements for the $BA_2MA_2Pb_3Br_4I_6$ film illuminated with continuous-wave UV light (λ = 365 nm, and I = 72 mW cm^{-2}) for 240 min are conducted. A set of patterns collected with a 40 min time interval reveals the simultaneous descent of peaks belonging to the quasi-2D phase and their shifting toward large angles (Figure 1b). Here, we find that the structural properties of the illuminated films do not recover under the dark conditions. Possible reasons for such irreversible behavior could be the sintering of perovskite units, divided by a large cation spacer, and the loss of iodide ions promoting the formation of exclusively Br-rich structural species having smaller lattice constants as compared to that of the initial mixed-halide perovskite. Finally, all of the peaks belonging to the quasi-2D phase completely disappear, and the XRD pattern appears very similar to that of the bulk ($n = \infty$) cubic $MAPbBr_3$ exhibiting signals at 2θ values of ∼15° and 30°, which correspond to the (100) and (200) planes, respectively (Figure 1b). A complete change in the XRD patterns is complemented by optical images of the sample emitting in the red range at the beginning of the experiment and green at the end (Figure S1).

The absorption spectrum of $BA_2PbBr_2I_2$ shows a strong exciton peak at 449 nm. With the increasing number of octahedral layers (n), this peak undergoes a bathochromic shift and becomes gradually less pronounced (Figure 1c). The former effect is caused by the band gap narrowing due to the reduction of quantum confinement in n = 2 and n = 3 layered RP phases, along with a slight increase in the I:Br ratio (R) taking the following values: 1 for n = 1, ∼1.33 for n = 2, and 1.50 for n = 3. The latter effect of the weakening of the exciton oscillator strength is related to the decrease in the exciton binding energy with an increase in both n and R. To establish some key energetic properties of the studied materials, we deconvolute the absorption spectra by using a function describing excitonic absorption[19] and, then, draw Tauc plots for band-to-band absorption (for details, see the Supporting Information and Figure S1). This gives us the following values for spectral broadening (Γ), exciton binding energy (E_b), and band gap energy (E_g): for n = 1, Γ = 0.11 eV, E_b = 0.22 eV, and E_g = 2.98 eV; for n = 2, Γ = −0.07, E_b = 0.17, and E_g = 2.62 eV, respectively; and for n = 3, Γ = −0.06 eV, E_b = 0.15 eV, and E_g = 2.45 eV, respectively. The descending trends for all of the values with an increase in n could be explained as follows. (i) An increase in the number of $[PbX_6]^{4-}$ octahedral layers gives more rigid structures that are more resistant to deformation of the crystal lattice and, hence, have a reduced number of defect states scattering excitons.[30] (ii) As the thickness of the 2D structure increases, the crystal lattice field more efficiently screens the photoexcited electron and hole from each other and, therefore, the exciton binding energy is decreasing.[31] (iii) The reduction of quantum confinement in n = 2 and n = 3 layered phases along with the increase in the I:Br ratio results in band gap narrowing. With regard to the latter, the band gap energy value for $BA_2MA_2Pb_3Br_4I_6$ (n = 3) is found to be much larger than that of bulk $MAPbBrI_2$ ($n \rightarrow \infty$), which is close to 1.8 eV.[32]

Next, the PL spectral evolution for the samples is systematically studied upon illumination under a 360 nm UV lamp with an intensity of 160 mW cm^{-2}. The n = 1 films exhibit a single green emission peak at 500 nm that slowly shifts toward 510 nm over the whole time interval of exposure to UV light (Figure 1d). Interestingly, here the spectral positions of this emission and the exciton absorption peak (Figure 1c) are very different and the Stokes shift, which is supposed to be small in quasi-2D perovskites,[33] is unusually large in this case. We assume that a reasonable explanation for

https://doi.org/10.1021/acs.jpclett.3c03151
J. Phys. Chem. Lett. 2024, 15, 540−548

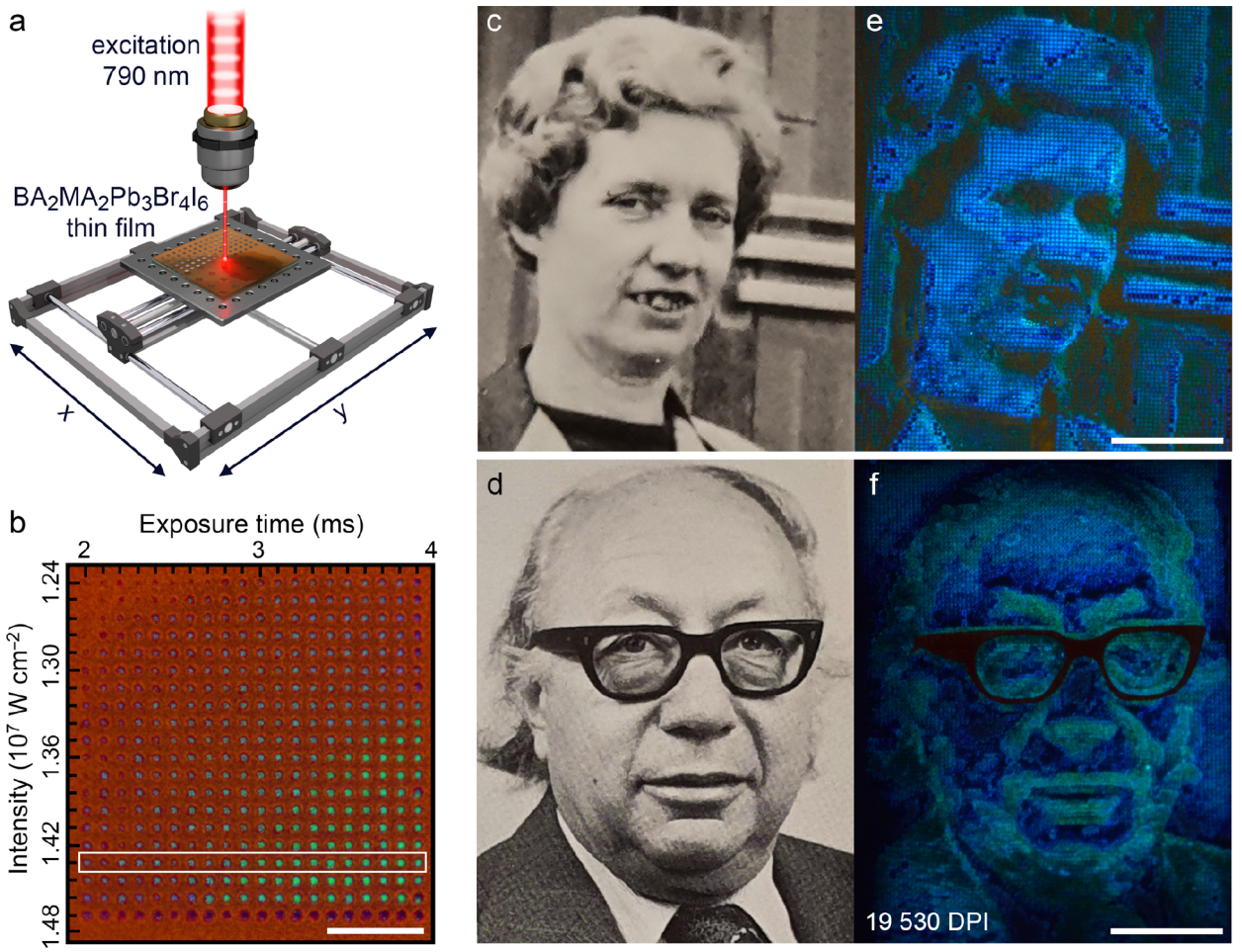

Figure 2. (a) Schematic illustration of a two-photon direct laser writing (DLW) procedure applied to the n = 3 quasi-2D perovskite thin film. (b) Luminescent image of an array of microspots preliminarily exposed to various intensities of 790 nm pulsed laser irradiation for various time intervals (scale bar of 50 μm). The white rectangle identifies an optimal dynamic range for DLW giving the widest PL color gamut with no burnt (overexposed) or poorly resolved (underexposed) spots. Original pictures of (c) Dr. S. Ruddlesden and (d) Prof. P. Popper chosen for the production of the corresponding high-resolution (19500 DPI) multicolor luminescent microimages (e and f, respectively) created by using the DLW method (scale bar of 50 μm). Photographs published with permission. Copyright 2021 Lucideon Ltd.

this observation could be an energy transfer process. In particular, we reckon that excitons formed in the n = 1 phase transfer to the one with the highest n formed at grain boundaries and experience radiative recombination.[34,35] Thus, traces of the low-band gap high-n phase possibly act as excitonic funnels. When we take this into account, it is not surprising that neither the XRD patterns nor the absorption spectra demonstrate the presence of the high-n phase in the $BA_2PbBr_2I_2$ film. The n = 2 and n = 3 films reveal similar the temporal behavior of the PL signal. Initially, they emit orange light at ∼560 nm, undergoing a gradual red-shift to ∼600 nm for 1000 s (Figure 1e,f), with the halide segregation phenomenon being responsible for such a clearly observable change.[20] The segregation leads to the formation of Br-rich and I-rich quasi-2D nanoscopic domains in perovskite films. The band gap of the latter is lower than that of the former, and thus, the latter domains play an active part in the exciton funneling process. It should be pointed out that PL from the I-rich phase slowly deteriorates with time. This happens because of the dissociation of the I-rich domains invoked by the $2I^- + 2h^+ \rightarrow I_2(g)$ reaction describing the generation of a volatile iodine species via the oxidation of iodide ions by photoexcited holes (h^+) in the valence band of perovskites.[36] To find evidence of such a dissociation mechanism, the n = 3 $BA_2MA_2Pb_3Br_4I_6$ film encapsulated together with a small piece of a KI test paper is illuminated until the reddish-orange luminescence completely deteriorates (Figure S3). One can see that the released I_2 gas reacts with KI, giving a darkened edge of the test paper beside the area of the film exposed to UV light for 100 min (bottom image in Figure S3). When the I-rich domains are finally depleted, exciton radiative recombination occurs within the Br-rich ones. Therefore, for the n = 2 film, we observe a peak at 434 nm assigned to $BA_2MAPb_2Br_7$[24] accompanied by the second peak at 454 nm, most likely related to the emission from hollow perovskite structures[37] containing large BA cations sealed in the $MAPbBr_3$ crystal lattice. These hollow perovskites are an intermediate of the sintering process, which are formed as a result of the evolution of the n = 3 film, along with the second less pronounced emission peak at 468 nm that belongs to the $BA_2MA_2Pb_3Br_{10}$ phase.[35] Finally, the blue emission in both n = 2 and n = 3 films changes to green, which occurs within the Br-rich quasi-2D domains due to the sintering process and results in the formation of phases with larger n values and finally bulk $MAPbBr_3$ ($n = \infty$) at the end. To illustrate the discussion presented above, a qualitative energy diagram (Figure 1g) visualizes three key stages during

https://doi.org/10.1021/acs.jpclett.3c03151
J. Phys. Chem. Lett. 2024, 15, 540−548

the evolution of the PL color governed by the aforementioned UV light-induced structural transformations of the $n = 2$ and $n = 3$ perovskite films.

To find more evidence of the proposed mechanism, we demonstrate synchronous absorption PL dynamics for all of the films (Figure S4). First, we measure the initial absorption spectra for them, and then, the samples are illuminated with UV light (λ_{ex} = 360 nm, and I = 160 mW cm^{-2}) to obtain PL dynamics. By interrupting the exposure of the films to UV light at certain moments and measuring absorption spectra for them, we collect consistent data on absorption and PL dynamics. It is established that the $n = 1$ film exhibits the following changes in its absorption spectrum (Figure S4a). (i) The absorption peak at 449 nm decreases and undergoes a blue-shift. (ii) A shoulder appears in the range of 500−520 nm and further evolves into a pronounced peak at 510 nm. (iii) A new peak at ∼400 nm arises. The first two observations are in good agreement with the halide segregation phenomenon, dissociation of the I-rich phase due to the release of I_2 species, and the formation of the bulk perovskite, whereas the third one can be explained by the formation of the BA_2PbBr_4 phase that exhibits its own excitonic absorption.[38] With regard to the PL dynamics for the $n = 1$ film (Figure S4b), we emphasize it is not capable of providing clear information about structural transformations because long-range exciton transport in quasi-2D perovskites[33] and efficient energy funneling phenomena[39] result in photoluminescence of the bulk phase impurity evenly distributed in the film. On the contrary, the absorption and PL dynamics for the $n = 2$ and $n = 3$ films look quite consistent. In particular, after the halide segregation and dissociation of the I-rich phase, in both absorption and PL spectra the peaks assigned to $BA_2MAPb_2Br_7$ (λ_{abs} = 430 nm and λ_{em} = 434 nm for the $n = 2$ film in Figure S4c,d)[38] and, most likely, to hollow perovskite structures (λ_{abs} = 450 nm and λ_{em} = 454 nm for the $n = 2$ and $n = 3$ films in Figure S4c−f)[37] can be clearly identified.

The evolution of PL spectra for the studied thin films can be captured well and conveniently represented in the form of shifting emission color coordinates according to the CIE 1931 color space diagram (Figure 1h). While the $n = 1$ sample shows no significant color change, the PL color for the $n = 2$ and $n = 3$ films starts from yellow (x = 0.395, y = 0.557) and orange (x = 0.559, y = 0.435), moving to purple (x = 0.167, y = 0.110) and blue (x = 0.131, y = 0.096), respectively, and finally turns to the same green color (x = 0.141, y = 0.775) on the color gamut. It should be noted that both of these phases experience a segregation-driven color change expressed in saturated orange hues (x = 0.441, y = 0.476) for the $n = 2$ film and (x = 0.591, y = 0.402) for the $n = 3$ film during the initial stage of excitation. It is important that the $n = 3$ phase displays the widest color span, which extends beyond the rec. 2020 (UHDTV) color space and, hence, is preferable for the production of optical data storage devices and optical writing of anticounterfeit images. The spectral evolution of the $n = 2$ phase is faster than that of the former, and the $n = 2$ phase could provide optical images with an additional degree of security related to the limited number of reading cycles. In the following, we demonstrate the realization of both opportunities.

Experimental data on the evolution of the PL color for the $n = 3$ quasi-2D perovskite films upon prolonged UV light illumination (see Figure 1h) inspire and justify their applicability to the production of multicolor PL patterns through the spatially resolved automatic management of the irradiation dose (fluence). One of the state-of-the-art techniques for the creation of such patterns is direct laser writing (DLW),[8] schematically illustrated in Figure 2a. To implement DLW on the $n = 3$ phase, we employ a lithography setup (for details, see Methods) based on a femtosecond pulsed Ti:sapphire laser (λ_{ex} = 790 nm, τ = 100 fs, and f = 80 MHz). Using this DLW system, the aforementioned photo-induced structural transformation from the quasi-2D to three-dimensional (3D) perovskite phase occurs because of the two-photon absorption phenomenon in the near-infrared range.[40] The irradiation dose can be conveniently controlled by varying two parameters: the intensity of the optical excitation and the duration of the exposure of the film to laser pulses. The dynamic range (DR) for the dosage is established as follows. At an intensity varying from 1.24×10^7 to 1.47×10^7 W cm^{-2}, the time interval of exposure varies in the range of 2.0−3.9 ms and, subsequently, the optimal set of produced luminescent pixels is selected (Figure 2b). Inspection of a whole array of the pixels depicted in Figure 2b reveals that the optimal DR spans from 2.86×10^4 to 5.75×10^4 J cm^{-2}, as this range does not result in any burnt (overexposed) or poorly resolved (underexposed) pixels.

Thereafter, we conduct the dots per inch (DPI) test to evaluate the maximum capacity of information produced by the DLW procedure. A bright-field microimage (Figure S5a) visualizing a set of 2 dot × 2 dot patterns reveals that the dots with a diameter of 1 μm can be spatially resolved when the distance between their centers is equal to 1.6 μm. This provides us with a maximum resolution of ∼19500 DPI a resolution at which we show the construction of a simple quick response (QR) code consisting of pixels emitting the same blue light (Figure S5b,c). The maximum resolution is also further used for the creation of complex multicolor micro-images.

To demonstrate the applicability of the $n = 3$ perovskite film to optical data storage and anticounterfeit labeling, two black and white pictures of the discoverers of the quasi-2D phase, Dr. Sheila Ruddlesden and Prof. Paul Popper (Figure 2c,d), are reproduced on a microscale. For this purpose, their photos are digitized and then downsampled to 20 shades of gray. Pixels possessing the lightest shade specify the regions to be subjected to the largest irradiation dose for parts of the film resulting in a green color of PL, whereas those with the darkest shade indicate the unexposed area exhibiting a reddish-orange PL. The rest of the shades set up a linear increment of the fluence in the range of 0−5.75×10^4 J cm^{-2}. As a result, corresponding multicolor high-resolution fluorescence images are formed (Figure 2d,f). These images provide reasonable examples of high-capacity optical data storage because each of the 20 shades encodes the corresponding PL spectrum, which could be assigned to a certain binary number. Furthermore, the spatial distribution of the resultant luminescent pixels makes it possible to consider such images as microscale anticounterfeit labels.

Following the trend of technological diversification for manufacturing luminescent microlabels, we examine a simple projection optical lithography (POL) instead of DLW. For this purpose, a mask with a logo of ITMO University consisting of a patterned aluminum film on a glass substrate is mounted before a 50× objective and shades a continuous-wave beam of UV light at 360 nm projected on the top of the $n = 2$ quasi-2D film (Figure 3a). At an incident light intensity of 3.5 W cm^{-2},

https://doi.org/10.1021/acs.jpclett.3c03151
J. Phys. Chem. Lett. 2024, 15, 540−548

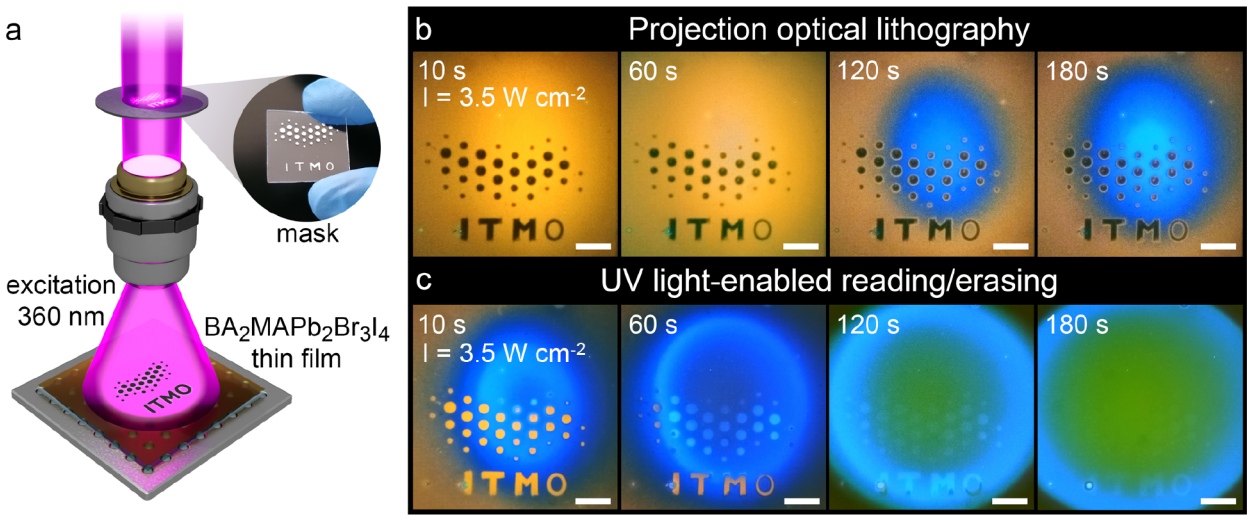

Figure 3. (a) Schematic illustration of the projection optical lithography procedure applied to the n = 2 quasi-2D perovskite thin film. (b) Luminescent images of the area exposed through a mask (with a logo of ITMO University) to focused UV light with an intensity of 3.5 W cm^{-2} for 10, 60, 120, and 180 s (scale bar of 50 μm). Black areas are shaded with the mask. Note that a blue luminescent spot appears in the center of the area because of the uneven distribution of the incident light intensity over the field of view. (c) Luminescent images of the same area after mask removal upon the same photoexcitation for 10, 60, 120, and 180 s. In the beginning of the visualization process, a contrast yellow pattern within the blue spot is revealed, which gradually disappears over time and finally turns to green.

the illuminated area shown in Figure 3b becomes blue in the center after 120 s because of the uneven lateral distribution of the irradiation. After mask removal, unexposed regions exhibit yellow luminescence and turn blue after illumination for 60 s (Figure 3c). Remarkably, more prolonged exposure to UV light (>120 s) causes erasure of the label, which manifests in the appearance of a green spot undergoing temporal lateral propagation (Figure 3c). Time intervals for writing and erasing steps can be controlled by tuning both the excitation intensity and the thickness of the studied quasi-2D film. Such behavior of the n = 2 phase is favorable for advanced security labeling,[41,42] which limits the number of label examination acts to only a few or even just one, making it invalid for further reading.

Finally, we study the resistance of encapsulated microimages and films to photobleaching caused by long-lasting light exposure to evaluate their applicability for storage on the shelf. For this purpose, a microimage encapsulated under ambient conditions (relative humidity of 35%) by using double-sided tape and a 150 μm thick coverslip is aged on a windowsill for 1 month. Thus, it is exposed to indoor lighting and direct sunlight in an ad hoc fashion at temperatures varying in the range of 20−40 °C. A comparison of pictures taken of the as-prepared microimage and the aged one shows no significant change (Figure S6a,b). Furthermore, we measure the absorption and PL spectral dynamics for samples encapsulated under the same conditions of the n = 3 thin film illuminated by continuous-wave UV light (λ_{ex} = 365 nm, and I = 80 mW cm^{-2}) for 600 min (Figure S6c,d). It is established that the encapsulated sample demonstrates the deceleration of the spectral dynamics by >40 times as compared to that of the non-encapsulated one irradiated by 2 times more intense light (Figure S4e,f). Importantly, the spectral dynamics for the n = 3 film encapsulated with KI test paper is ∼15 times faster than that of one without it (Figure S7). We assume the reason for such a drastic difference in dynamics stems from the ability of released I_2 species to react with the film and, hence, to decelerate the conversion of the mixed-halide quasi-2D phase into the pure bromide quasi-2D one. Therefore, in the presence of KI test paper absorbing I_2, the conversion accelerates. Thus, the I_2 release process is recognized as being responsible for the most pronounced change in the PL color of our samples. A further change in the PL color caused by the light-induced transition from the pure bromide quasi-2D phase to the bulk perovskite could be assisted by oxygen or/and moisture or could be a thermally assisted process. Considering all of this, one can see how even a very simple encapsulation procedure substantially increases the temporal stability of the luminescent microimages and films and provides them with an opportunity for commercialization.

In summary, we have demonstrated the light-induced PL emission tuning of $BA_2MA_{n-1}Pb_n(Br,I)_{3n+1}$ (n = 2 and 3) thin films. The mechanisms for such spectral tuning in the studied mixed-halide quasi-2D Ruddlesden−Popper perovskites involve irreversible compositional and structural modifications, which go beyond the conventional halide segregation in 3D (bulk) perovskites. It has been established that the n = 3 film is more resistant to the light-driven transition from the quasi-2D phase to the 3D bulk phase than is the n = 2 film. This has allowed us to create high-resolution multicolor microimages on the n = 3 quasi-2D perovskite thin films using a two-photon direct laser writing method by controlling the irradiation dose and exposure time. These images can be considered as examples of high-capacity optical data storage and could meet the demands of information encryption technology, which significantly exceeds previous works on halide perovskites in terms of DPI.[43−46] Moreover, a simple projection UV lithography has been applied to the n = 2 quasi-2D perovskite films to demonstrate light-erasable luminescent labels, which may provide secure items with an advanced level of protection and accelerate the potential progress in anticounterfeiting. A further increase in resolution can be achieved by integration of the quasi-2D perovskites with various optically resonant nanostructures localizing and amplifying light at the nanoscale.[47−52]

https://doi.org/10.1021/acs.jpclett.3c03151
J. Phys. Chem. Lett. 2024, 15, 540−548

METHODS

Fabrication of Quasi-2D Perovskite Thin Films. Lead halide RP phase precursor solutions were obtained by mixing 138.3 mg (0.3 mmol) of lead(II) iodide (PbI_2, TCI, 99.99%, trace metals basis) with the corresponding amounts of methylammonium bromide (MABr, Greatcell Solar, 99.99%) and/or *n*-butylammonium bromide (BABr, Greatcell Solar, 98%) and dissolution of the mixtures in 1 mL of anhydrous dimethyl sulfoxide (DMSO, Sigma-Aldrich, 99.9%). For the $BA_2PbBr_2I_2$ (n = 1) solution, 92.4 mg (0.6 mmol) of BABr was used. For the $BA_2MAPb_2Br_3I_4$ (n = 2) solution, 46.2 mg (0.3 mmol) of BABr and 16.8 mg (0.15 mmol) of MABr were employed. For the $BA_2MA_2Pb_3Br_4I_6$ (n = 3) solution, 30.8 mg (0.2 mmol) of BABr and 22.4 mg (0.2 mmol) of MABr were used. Glass substrates were cleaned by subsequent ultrasonication in acetone and 2-propanol, rinsed with deionized water, and exposed to ozone treatment for 10 min to improve the wettability of the surface. The precursor solutions were spin-casted on the substrates at 2500 rpm for 5 min and then annealed on a hot plate at 60 °C for 5 min. The thickness of the resulting thin films was 60 nm. All of the procedures were conducted inside a N_2-filled glovebox with both O_2 and H_2O concentrations (not exceeding 1 ppm).

Characterization of Thin Films. The thickness of the deposited films was measured by using a Tencor P-7 stylus profilometer (KLA). Optical absorption spectra were recorded by using a model UV-3600 spectrophotometer (Shimadzu). XRD patterns of the samples were measured in θ–θ geometry on a SmartLab diffractometer (Rigaku) equipped with a 9 kW rotating Cu anode X-ray tube. Bright-field and fluorescence images of the samples were obtained on an Axio Imager A2m (Carl Zeiss) microscope with 50× and 100× objectives (Carl Zeiss EC Epiplan-NEOFLUAR). The evolution of PL spectra was recorded using a QE Pro optical fiber spectrometer (Ocean Optics) coupled with the microscope in fluorescence mode.

Direct Laser Writing. For creating various micropatterns on the perovskite film surface, the direct laser writing (DLW) technique was applied. Laser pulses with a duration of 100 fs from a Ti-sapphire oscillator emitting at a wavelength of 790 nm with a repetition rate of 80 MHz were focused through a 40× objective (NA = 0.7) onto the quasi-2D perovskite film surface. The irradiation power was monitored with a thermopile sensor and controlled by a motorized half-wave plate ($\lambda/2$) and a polarizing beamsplitter. The exposure time was controlled by an acousto-optical modulator used as a fast laser shutter. The positioning of the sample was performed by air bearing linear motor stages (Aerotech). DLW was conducted under ambient conditions (relative humidity of 35%).

Projection UV Optical Lithography. A thin-film (100 nm) metal pattern on a glass substrate was fabricated by thermal evaporation of aluminum pellets (Ted Pella, Inc., 99.999%) with a deposition rate of 0.3 nm s^{-1} in a vacuum chamber (Kurt J Lesker Co.) at 2×10^{-7} Torr. The obtained mask with a logo of ITMO University was mounted on the microscope instead of an aperture-adjustable optical iris diaphragm in front of an HBO 100 W/2 mercury short-arc lamp (OSRAM). The optical power of the focused incident UV light was measured with a Star Bright power meter (Ophir Photonics). Projection UV optical lithography was conducted under ambient conditions (relative humidity of 35%).

ASSOCIATED CONTENT

Supporting Information

The Supporting Information is available free of charge at https://pubs.acs.org/doi/10.1021/acs.jpclett.3c03151.

Photographs of the n = 3 quasi-2D perovskite film at the beginning and end of *in situ* XRD measurement, pictures of the n = 3 film examined for I_2 gas release, bright-field and luminescence microimages of 2 dot × 2 dot patterns, and high-resolution QR code produced by using the two-photon DLW method (PDF)

Transparent Peer Review report available (PDF)

AUTHOR INFORMATION

Corresponding Authors

Anatoly P. Pushkarev − *ITMO University, 197101 St. Petersburg, Russia;* orcid.org/0000-0002-1793-6812; Email: anatoly.pushkarev@metalab.ifmo.ru

Sergey V. Makarov − *ITMO University, 197101 St. Petersburg, Russia; Qingdao Innovation and Development Center, Harbin Engineering University, Qingdao 266000 Shandong, P. R. China;* orcid.org/0000-0002-9257-6183; Email: s.makarov@metalab.ifmo.ru

Authors

Sergey S. Anoshkin − *ITMO University, 197101 St. Petersburg, Russia*

Ivan I. Shishkin − *ITMO University, 197101 St. Petersburg, Russia;* orcid.org/0000-0002-2330-0159

Daria I. Markina − *ITMO University, 197101 St. Petersburg, Russia*

Lev S. Logunov − *ITMO University, 197101 St. Petersburg, Russia*

Hilmi Volkan Demir − *UNAM-Institute of Materials Science and Nanotechnology, National Nanotechnology Research Center, Department of Electrical and Electronics Engineering, Department of Physics, Bilkent University, Ankara 06800, Turkey; LUMINOUS! Center of Excellence for Semiconductor Lighting and Displays, School of Electrical and Electronic Engineering, School of Physical and Materials Sciences, School of Materials Science and Nanotechnology, Nanyang Technological University, Singapore 639798;* orcid.org/0000-0003-1793-112X

Andrey L. Rogach − *Department of Materials Science and Engineering and Centre for Functional Photonics (CFP), City University of Hong Kong, Kowloon, Hong Kong SAR 999077, P. R. China; Qingdao Innovation and Development Center, Harbin Engineering University, Qingdao 266000 Shandong, P. R. China;* orcid.org/0000-0002-8263-8141

Complete contact information is available at: https://pubs.acs.org/10.1021/acs.jpclett.3c03151

Notes

The authors declare no competing financial interest.

ACKNOWLEDGMENTS

This research was supported by the Priority 2030 Federal Academic Leadership Program and by the Croucher Foundation of the Hong Kong SAR. H.V.D. gratefully acknowledges support from TUBA. S.V.M. aknowledges National Natural Science Foundation of China (project 62350610272). The authors thank Dr. Vidas Pakštas for measuring XRD patterns (Figure [1,]b). The authors are grateful

to Ann Pace (Lucideon Ltd.) for providing them with pictures of Dr. S. Ruddlesden and Prof. P. Popper. The authors thank Mr. Ivan Pustovit for assistance in graphic design.

REFERENCES

(1) Tsai, W.-P.; Feng, D.; Pan, M.; Beck, H.; Lawson, K.; Yang, Y.; Liu, J.; Shen, C. From Calibration to Parameter Learning: Harnessing the Scaling Effects of Big Data in Geoscientific Modeling. *Nat. Commun.* **2021**, *12*, 5988.

(2) Lemm, D.; von Rudorff, G. F.; von Lilienfeld, O. A. Machine Learning Based Energy-Free Structure Predictions of Molecules, Transition States, and Solids. *Nat. Commun.* **2021**, *12*, 4468.

(3) Plata, D. L.; Janković, N. Z. Achieving Sustainable Nanomaterial Design Though Strategic Cultivation of Big Data. *Nat. Nanotechnol.* **2021**, *16*, 612−614.

(4) Lee, B.; Yoon, S.; Lee, J. W.; Kim, Y.; Chang, J.; Yun, J.; Ro, J. C.; Lee, J.-S.; Lee, J. H. Statistical Characterization of The Morphologies of Nanoparticles Through Machine Learning Based Electron Microscopy Image Analysis. *ACS Nano* **2020**, *14*, 17125−17133.

(5) Jiang, P.; Sinha, S.; Aldape, K.; Hannenhalli, S.; Sahinalp, C.; Ruppin, E. Big Data in Basic and Translational Cancer Research. *Nat. Rev. Cancer* **2022**, *22*, 625−639.

(6) Huang, X.; Guo, Q.; Yang, D.; Xiao, X.; Liu, X.; Xia, Z.; Fan, F.; Qiu, J.; Dong, G. Reversible 3D Laser Printing of Perovskite Quantum Dots Inside a Transparent Medium. *Nat. Photonics* **2020**, *14*, 82−88.

(7) Zhizhchenko, A. Y.; Tonkaev, P.; Gets, D.; Larin, A.; Zuev, D.; Starikov, S.; Pustovalov, E. V.; Zakharenko, A. M.; Kulinich, S. A.; Juodkazis, S.; Kuchmizhak, A. A.; Makarov, S. V. Light-Emitting Nanophotonic Designs Enabled by Ultrafast Laser Processing of Halide Perovskites. *Small* **2020**, *16*, 2000410.

(8) Zhan, W.; Meng, L.; Shao, C.; Wu, X.-g.; Shi, K.; Zhong, H. In Situ Patterning Perovskite Quantum Dots by Direct Laser Writing Fabrication. *ACS Photonics* **2021**, *8*, 765−770.

(9) Sun, K.; Tan, D.; Fang, X.; Xia, X.; Lin, D.; Song, J.; Lin, Y.; Liu, Z.; Gu, M.; Yue, Y.; Qiu, J. Three-Dimensional Direct Lithography of Stable Perovskite Nanocrystals in Glass. *Science* **2022**, *375*, 307−310.

(10) Cheng, C.-H.; Yang, D. S.; Kim, J.; Deotare, P. B. Self-Erasable and Rewritable Optoexcitonic Platform for Antitamper Hardware. *Adv. Opt. Mater.* **2020**, *8*, 2001287.

(11) Gong, X.; Qiao, Z.; Liao, Y.; Zhu, S.; Shi, L.; Kim, M.; Chen, Y.-C. Enzyme-Programmable Microgel Lasers for Information Encoding and Anti-Counterfeiting. *Adv. Mater.* **2022**, *34*, 2107809.

(12) Larin, A. O.; Dvoretckaia, L. N.; Mozharov, A. M.; Mukhin, I. S.; Cherepakhin, A. B.; Shishkin, I. I.; Ageev, E. I.; Zuev, D. A. Luminescent Erbium-Doped Silicon Thin Films for Advanced Anti-Counterfeit Labels. *Adv. Mater.* **2021**, *33*, 2005886.

(13) Haeger, T.; Heiderhoff, R.; Riedl, T. Thermal Properties of Metal-Halide Perovskites. *J. Mater. Chem. C* **2020**, *8*, 14289−14311.

(14) Zhizhchenko, A.; Syubaev, S.; Berestennikov, A.; Yulin, A. V.; Porfirev, A.; Pushkarev, A.; Shishkin, I.; Golokhvast, K.; Bogdanov, A. A.; Zakhidov, A. A.; Kuchmizhak, A. A.; Kivshar, Y. S.; Makarov, S. V. Single-Mode Lasing from Imprinted Halide-Perovskite Microdisks. *ACS Nano* **2019**, *13*, 4140−4147.

(15) Zhizhchenko, A.; Cherepakhin, A.; Masharin, M.; Pushkarev, A.; Kulinich, S.; Porfirev, A.; Kuchmizhak, A.; Makarov, S. Direct Imprinting of Laser Field on Halide Perovskite Single Crystal for Advanced Photonic Applications. *Laser Photonics Rev.* **2021**, *15*, 2100094.

(16) Zhizhchenko, A. Y.; Cherepakhin, A. B.; Masharin, M. A.; Pushkarev, A. P.; Kulinich, S. A.; Kuchmizhak, A. A.; Makarov, S. V. Directional Lasing from Nanopatterned Halide Perovskite Nanowire. *Nano Lett.* **2021**, *21*, 10019−10025.

(17) Wang, Z.; Yang, T.; Zhang, Y.; Ou, Q.; Lin, H.; Zhang, Q.; Chen, H.; Hoh, H. Y.; Jia, B.; Bao, Q. Flat Lenses Based on 2D Perovskite Nanosheets. *Adv. Mater.* **2020**, *32*, 2001388.

(18) Protesescu, L.; Yakunin, S.; Bodnarchuk, M. I.; Krieg, F.; Caputo, R.; Hendon, C. H.; Yang, R. X.; Walsh, A.; Kovalenko, M. V. Nanocrystals of Cesium Lead Halide Perovskites ($CsPbX_3$, X= Cl, Br, and I): Novel Optoelectronic Materials Showing Bright Emission with Wide Color Gamut. *Nano Lett.* **2015**, *15*, 3692−3696.

(19) Liashenko, T. G.; Cherotchenko, E. D.; Pushkarev, A. P.; Pakštas, V.; Naujokaitis, A.; Khubezhov, S. A.; Polozkov, R. G.; Agapev, K. B.; Zakhidov, A. A.; Shelykh, I. A.; Makarov, S. V. Electronic Structure of $CsPbBr_{3-x}Cl_x$ Perovskites: Synthesis, Experimental Characterization, and DFT Simulations. *Phys. Chem. Chem. Phys.* **2019**, *21*, 18930−18938.

(20) Hoke, E. T.; Slotcavage, D. J.; Dohner, E. R.; Bowring, A. R.; Karunadasa, H. I.; McGehee, M. D. Reversible Photo-Induced Trap Formation in Mixed-Halide Hybrid Perovskites for Photovoltaics. *Chem. Sci.* **2015**, *6*, 613−617.

(21) Brennan, M. C.; Draguta, S.; Kamat, P. V.; Kuno, M. Light-Induced Anion Phase Segregation in Mixed Halide Perovskites. *ACS Energy Lett.* **2018**, *3*, 204−213.

(22) Knight, A. J.; Wright, A. D.; Patel, J. B.; McMeekin, D. P.; Snaith, H. J.; Johnston, M. B.; Herz, L. M. Electronic Traps and Phase Segregation in Lead Mixed-Halide Perovskite. *ACS Energy Lett.* **2019**, *4*, 75−84.

(23) Ha, S. K.; Mauck, C. M.; Tisdale, W. A. Toward stable deep-blue luminescent colloidal lead halide perovskite nanoplatelets: systematic photostability investigation. *Chem. Mater.* **2019**, *31*, 2486−2496.

(24) Leung, T. L.; Tam, H. W.; Liu, F.; Lin, J.; Ng, A. M. C.; Chan, W. K.; Chen, W.; He, Z.; Lončarić, I.; Grisanti, L.; Ma, C.; Wong, K. S.; Lau, Y. S.; Zhu, F.; Skoko, Ž.; Popović, J.; Djurišić, A. B. Mixed Spacer Cation Stabilization of Blue-Emitting n= 2 Ruddlesden−Popper Organic−Inorganic Halide Perovskite Films. *Adv. Opt. Mater.* **2020**, *8*, 1901679.

(25) Sen, A.; Chatterjee, S.; Sen, P. UV-Assisted Conversion of 2D Ruddlesden−Popper Iodide Perovskite Nanoplates into Stable 3D $MAPbI_3$ Nanorods. *J. Phys. Chem. C* **2022**, *126*, 18057−18066.

(26) Gan, Z.; Cheng, Y.; Chen, W.; Loh, K. P.; Jia, B.; Wen, X. Photophysics of 2D Organic−Inorganic Hybrid Lead Halide Perovskites: Progress, Debates, and Challenges. *Adv. Sci.* **2021**, *8*, 2001843.

(27) Solanki, A.; Guerrero, A.; Zhang, Q.; Bisquert, J.; Sum, T. C. Interfacial Mechanism for Efficient Resistive Switching in Ruddlesden−Popper Perovskites for Non-Volatile Memories. *J. Phys. Chem. Lett.* **2020**, *11*, 463−470.

(28) Tian, Q.; Hong, R.; Liu, C.; Hong, X.; Zhang, S.; Wang, L.; Lv, Y.; Liu, X.; Zou, X.; Liao, L. Flexible SnO Optoelectronic Memory Based on Light-Dependent Ionic Migration in Ruddlesden−Popper Perovskite. *Nano Lett.* **2022**, *22*, 494−500.

(29) Stoumpos, C. C.; Cao, D. H.; Clark, D. J.; Young, J.; Rondinelli, J. M.; Jang, J. I.; Hupp, J. T.; Kanatzidis, M. G. Ruddlesden−Popper Hybrid Lead Iodide Perovskite 2D Homologous Semiconductors. *Chem. Mater.* **2016**, *28*, 2852−2867.

(30) Cortecchia, D.; Neutzner, S.; Srimath Kandada, A. R.; Mosconi, E.; Meggiolaro, D.; De Angelis, F.; Soci, C.; Petrozza, A. Broadband emission in two-dimensional hybrid perovskites: the role of structural deformation. *J. Am. Chem. Soc.* **2017**, *139*, 39−42.

(31) Chernikov, A.; Berkelbach, T. C.; Hill, H. M.; Rigosi, A.; Li, Y.; Aslan, B.; Reichman, D. R.; Hybertsen, M. S.; Heinz, T. F. Exciton binding energy and nonhydrogenic Rydberg series in monolayer WS_2. *Phys. Rev. Lett.* **2014**, *113*, 076802.

(32) Cui, D.; Yang, Z.; Yang, D.; Ren, X.; Liu, Y.; Wei, Q.; Fan, H.; Zeng, J.; Liu, S. Color-tuned perovskite films prepared for efficient solar cell applications. *J. Phys. Chem. C* **2016**, *120*, 42−47.

(33) Deng, S.; Shi, E.; Yuan, L.; Jin, L.; Dou, L.; Huang, L. Long-Range Exciton Transport and Slow Annihilation in Two-Dimensional Hybrid Perovskites. *Nat. Commun.* **2020**, *11*, 664.

(34) Qin, Z.; Dai, S.; Gajjela, C. C.; Wang, C.; Hadjiev, V. G.; Yang, G.; Li, J.; Zhong, X.; Tang, Z.; Yao, Y.; Guloy, A. M.; Reddy, R.; Mayerich, D.; Deng, L.; Yu, Q.; Feng, G.; Calderon, H. A.; Robles-Hernandez, F. C.; Wang, Z. M.; Bao, J. Spontaneous Formation of 2D/3D Heterostructures on the Edges of 2D Ruddlesden−Popper Hybrid Perovskite Crystals. *Chem. Mater.* **2020**, *32*, 5009−5015.

https://doi.org/10.1021/acs.jpclett.3c03151
J. Phys. Chem. Lett. 2024, 15, 540−548

(35) Qin, Y.; Li, Z.-G.; Gao, F.-F.; Chen, H.; Li, X.; Xu, B.; Li, Q.; Jiang, X.; Li, W.; Wu, X.; Quan, Z.; Ye, L.; Zhang, Y.; Lin, Z.; Pedesseau, L.; Even, J.; Lu, P.; Bu, X.-H. Dangling Octahedra Enable Edge States in 2D Lead Halide Perovskites. *Adv. Mater.* **2022**, *34*, 2201666.
(36) Brennan, M. C.; Toso, S.; Pavlovetc, I. M.; Zhukovskyi, M.; Marras, S.; Kuno, M.; Manna, L.; Baranov, D. Superlattices are Greener on the Other Side: How Light Transforms Self-Assembled Mixed Halide Perovskite Nanocrystals. *ACS Energy Lett.* **2020**, *5*, 1465−1473.
(37) Worku, M.; Tian, Y.; Zhou, C.; Lin, H.; Chaaban, M.; Xu, L.-j.; He, Q.; Beery, D.; Zhou, Y.; Lin, X.; Su, Y.-F.; Xin, Y.; Ma, B. Hollow Metal Halide Perovskite Nanocrystals with Efficient Blue Emissions. *Sci. Adv.* **2020**, *6*, eaaz5961.
(38) Li, H.; Qin, Y.; Shan, B.; Shen, Y.; Ersan, F.; Soignard, E.; Ataca, C.; Tongay, S. Unusual pressure-driven phase transformation and band renormalization in 2D vdW hybrid lead halide perovskites. *Adv. Mater.* **2020**, *32*, 1907364.
(39) Lei, L.; Seyitliyev, D.; Stuard, S.; Mendes, J.; Dong, Q.; Fu, X.; Chen, Y.-A.; He, S.; Yi, X.; Zhu, L.; Chang, C.-H.; Ade, H.; Gundogdu, K.; So, F. Efficient energy funneling in quasi-2D perovskites: from light emission to lasing. *Adv. Mater.* **2020**, *32*, 1906571.
(40) Walters, G.; Sutherland, B. R.; Hoogland, S.; Shi, D.; Comin, R.; Sellan, D. P.; Bakr, O. M.; Sargent, E. H. Two-Photon Absorption in Organometallic Bromide Perovskites. *ACS Nano* **2015**, *9*, 9340−9346.
(41) Yu, J.; Luo, M.; Lv, Z.; Huang, S.; Hsu, H.-H.; Kuo, C.-C.; Han, S.-T.; Zhou, Y. Recent Advances in Optical and Optoelectronic Data Storage Based on Luminescent Nanomaterials. *Nanoscale* **2020**, *12*, 23391−23423.
(42) Zhuang, Y.; Ren, X.; Che, X.; Liu, S.; Huang, W.; Zhao, Q. Organic Photoresponsive Materials for Information Storage: a Review. *Adv. Photon.* **2021**, *3*, 014001.
(43) Zou, C.; Zheng, J.; Chang, C.; Majumdar, A.; Lin, L. Y. Nonvolatile rewritable photomemory arrays based on reversible phase-change perovskite for optical information storage. *Adv. Opt. Mater.* **2019**, *7*, 1900558.
(44) Zhou, C.; Cao, G.; Gan, Z.; Ou, Q.; Chen, W.; Bao, Q.; Jia, B.; Wen, X. Spatially Modulating the Fluorescence Color of Mixed-Halide Perovskite Nanoplatelets Through Direct Femtosecond Laser Writing. *ACS Appl. Mater. Interfaces* **2019**, *11*, 26017−26023.
(45) Minh, D. N.; Nguyen, L. A. T.; Trinh, C. T.; Oh, C.; Eom, S.; Vu, T. V.; Choi, J.; Sim, J. H.; Lee, K.-G.; Kim, J.; Cho, S. C.; Lee, S. U.; Cimrová, V.; Kang, Y. Low-Dimensional Single-Cation Formamidinium Lead Halide Perovskites ($FA_{m+2}Pb_mBr_{3m+2}$): From Synthesis to Rewritable Phase-Change Memory Film. *Adv. Funct. Mater.* **2021**, *31*, 2011093.
(46) Kanwat, A.; Ghosh, B.; Ng, S. E.; Rana, P. J.; Lekina, Y.; Hooper, T. J.; Yantara, N.; Kovalev, M.; Chaudhary, B.; Kajal, P.; Febriansyah, B.; Tan, Q. Y.; Klein, M.; Shen, Z. X.; Ager, J. W.; Mhaisalkar, S. G.; Mathews, N. Reversible photochromism in < 110> oriented layered halide perovskite. *ACS Nano* **2022**, *16*, 2942−2952.
(47) Schuller, J. A.; Barnard, E. S.; Cai, W.; Jun, Y. C.; White, J. S.; Brongersma, M. L. Plasmonics for extreme light concentration and manipulation. *Nature materials* **2010**, *9*, 193−204.
(48) Slobozhanyuk, A. P.; Ginzburg, P.; Powell, D. A.; Iorsh, I.; Shalin, A. S.; Segovia, P.; Krasavin, A. V.; Wurtz, G. A.; Podolskiy, V. A.; Belov, P. A.; et al. Purcell effect in hyperbolic metamaterial resonators. *Phys. Rev. B* **2015**, *92*, 195127.
(49) Kristensen, A.; Yang, J. K.; Bozhevolnyi, S. I.; Link, S.; Nordlander, P.; Halas, N. J.; Mortensen, N. A. Plasmonic colour generation. *Nat. Rev. Mater.* **2017**, *2*, 16088.
(50) Makarov, S.; Furasova, A.; Tiguntseva, E.; Hemmetter, A.; Berestennikov, A.; Pushkarev, A.; Zakhidov, A.; Kivshar, Y. Halide-perovskite resonant nanophotonics. *Adv. Opt. Mater.* **2019**, *7*, 1800784.
(51) Machnev, A. A.; Pushkarev, A. P.; Tonkaev, P.; Noskov, R. E.; Rusimova, K. R.; Mosley, P. J.; Makarov, S. V.; Ginzburg, P. B.; Shishkin, I. I. Modifying light−matter interactions with perovskite nanocrystals inside antiresonant photonic crystal fiber. *Photonics Research* **2021**, *9*, 1462−1469.
(52) Zhu, H.; Chu, L.; Liu, W.; Juodkazis, S.; Chen, F. Ultrafast Laser-Induced Plasmonic Modulation of Optical Properties of Dielectrics at High Resolution. *Adv. Opt. Mater.* **2023**, *11*, 2300929.

https://doi.org/10.1021/acs.jpclett.3c03151
J. Phys. Chem. Lett. 2024, 15, 540−548